

NASA CONTRACTOR REPORT

NASA-CR-196365

5-17
19566
3412

COMPUTATIONAL STUDIES OF METAL-METAL AND METAL-LIGAND INTERACTIONS

Leslie A. Barnes

Eloret Institute
3788 Fabian Way
Palo Alto, CA 94303

N95-10146
COMPUTATIONAL
STUDIES OF METAL-METAL AND
METAL-LIGAND INTERACTIONS Final
Technical Report, 1 Oct. 1991 - 30
Jun. 1994 (Eloret Corp.) 54 p
Unclassified

63/76 0019566

Prepared for

Ames Research Center
under Cooperative Agreement NCC2-741



National Aeronautics and
Space Administration

Ames Research Center
Moffett Field, California 94035

NASA CONTRACTOR REPORT

**COMPUTATIONAL STUDIES OF METAL-METAL
AND METAL-LIGAND INTERACTIONS**

Leslie A. Barnes

CONTRACT NAS2-



The following papers resulted from this research activity:

A (1) L.A. Barnes, B. Liu, and R. Lindh, "Bond Length, dipole moment and harmonic frequency of CO," J. Chem. Phys., **98**, 3972--3977, (1993).

OK (2) L.A. Barnes, B. Liu, and R. Lindh, "Structure and energetics of Cr(CO)₆ and Cr(CO)₅," J. Chem. Phys., **98**, 3978--3989, (1993). *10/4/93
2/12/94*

(3) Lindh and L.A. Barnes, "The Fraternal Twins of Quartet O₄⁺," J. Chem. Phys. **100**, 1, 224-237, (1994).

(4) L.A. Barnes and R. Lindh, "Symmetry Breaking in O₄⁺: an Application of the Brueckner Coupled Cluster Method," Chem. Phys. Lett., **223**, 207, (1994).

(5) L.A. Barnes, "A Multi-Region Integration Scheme," to be published.

Papers (3) to (5) were not included in earlier reports submitted under this Cooperative Agreement and are attached to this final technical report.

1. Report No.	2. Government Accession No.	3. Recipient's Catalog No.	
4. Title and Subtitle Computational Studies of Metal-Metal and Metal-Ligand Interactions		5. Report Date 22 July, 1994	
7. Author(s) Leslie A. Barnes		6. Performing Organization Code	
9. Performing Organization Name and Address		8. Performing Organization Report No.	
12. Sponsoring Agency Name and Address National Aeronautics and Space Administration, Washington, D.C. 20456		10. Work Unit No.	
15. Supplementary Notes Point of Contact: Dr. Stephen P. Langhoff c/o 230-2, NASA Ames Research Center, Moffett Field, CA 94035		11. Contract or Grant No. NCC2-741	
		13. Type of Report and Period Covered 10/1/91 to 6/30/94	
		14. Sponsoring Agency Code	
16. Abstract Accurate calculations on the bond length, dipole moment, and harmonic frequency of CO are presented, using large basis sets and high levels of electron correlation. The geometric structure, force constants and binding energies of Cr(CO) ₆ and Cr(CO) ₅ are computed using large basis sets and high levels of electron correlation. The molecule O ₄ ⁺ is studied, using large basis sets and high levels of electron correlation, including the CASSCF, CASSI and CASPT2 methods. Binding energies, geometries and frequencies are computed. Symmetry breaking is a particular problem for the antisymmetric stretch, which is addressed using the CASSI method. The symmetry breaking problem in O ₄ ⁺ has also been studied using the Brueckner coupled-cluster method. This gives results in good agreement with CASSI. A multi-region numerical integration scheme is investigated for use in Density Functional Calculations. This scheme is found to give comparable results to a widely used scheme based on the Euler-Maclaurin technique.			
17. Key Words (Suggested by Author(s)) Metal-Metal Interactions Metal-Ligand Interactions Electron Correlation Density Functional Calculations		18. Distribution Statement unclassified, unlimited	
19. Security Classif. (of this report) unclassified	20. Security Classif. (of this page) unclassified	21. No. of Pages	22. Price*

*For sale by the National Technical Information Service, Springfield, Virginia 22161

COMPUTATIONAL STUDIES OF METAL-METAL AND METAL-LIGAND INTERACTIONS

**Final Technical Report
for
Cooperative Agreement NCC2-741**

for the period
October 1, 1991 - June 30, 1994

Submitted to

National Aeronautics and Space Administration
Ames Research Center
Moffett Field, California 94035

Computational Chemistry Branch
Dr. Stephen R. Langhoff, Chief and Technical Officer

Thermosciences Division
Dr. James O. Arnold, Chief

Prepared by

ELORET INSTITUTE
3788 Fabian Way
Palo Alto, CA 94303
Phone: (415) 493-4710
Telfax: (415) 424-9876

Dr. K. Heinemann, President and Grant Administrator
Dr. Leslie A. Barnes, Principal Investigator

22 July, 1994

Accuracte calculations on the bond length, dipole moment and harmonic frequency of CO are presented, using large basis sets and high levels of electron correlation. The geometric structure, forceconstants and binding energies of Cr(CO)₆ and Cr(CO)₅ are computed using large basis sets and high levels of electron correlation. The molecule O₄⁺ is studied, using large basis sets and high levels of electron correlation, including CASSCF, CASSI and CASPT2 methods. Binding energies, geometries and frequencies are computed. Symmetry breaking is a particular problem for the antisymmetric stretch, which is addressed using the CASSI method. The symmetry breaking problem in O₄⁺ has also been studied using the Brueckner coupled-cluster method. This gives results in good agreement with CASSI. A multi-region numerical integration scheme is investigated for use in Density Functional Calculations. This scheme is found to give comparable results to a widely used scheme based on the Euler-Maclaurin technique.

- “Bond length, dipole moment and harmonic frequency of CO”, L. A. Barnes, B. Liu and R. Lindh, J. Chem. Phys., **98**, 3972–3977, (1993)

A detailed comparison of some properties of CO is given, at the modified coupled-pair functional (MCPF), single and double excitation coupled-cluster (CCSD) and CCSD(T) levels of theory (including a perturbational estimate for connected triple excitations), using a variety of basis sets. With very large one-particle basis sets, the CCSD(T) method gives excellent results for the bond distance, dipole moment and harmonic frequency of CO. In a [6s 5p 4d 3f 2g 1h] + (1s 1p 1d) basis set, the bond distance is about 0.005 a_0 too large, the dipole moment about 0.005 a.u. too small and the frequency about 6 cm^{-1} too small, when compared with experimental results.

- “Structure and energetics of $\text{Cr}(\text{CO})_6$ and $\text{Cr}(\text{CO})_5$ ”, L. A. Barnes, B. Liu and R. Lindh, J. Chem. Phys., **98**, 3978–3989, (1993)

The geometric structure of $\text{Cr}(\text{CO})_6$ is optimized at the modified coupled-pair functional (MCPF), single and double excitation coupled-cluster (CCSD) and CCSD(T) levels of theory (including a perturbational estimate for connected triple excitations), and the force constants for the totally symmetric representation are determined. The geometry of $\text{Cr}(\text{CO})_5$ is partially optimized at the MCPF, CCSD and CCSD(T) levels of theory. Comparison with experimental data shows that the CCSD(T) method gives the best

results for the structures and force constants, and that remaining errors are probably due to deficiencies in the one-particle basis sets used for CO. A detailed comparison of the properties of free CO is therefore given, at both the MCPF and CCSD/CCSD(T) levels of treatment, using a variety of basis sets. With very large one-particle basis sets, the CCSD(T) method gives excellent results for the bond distance, dipole moment and harmonic frequency of free CO. The total binding energies of Cr(CO)₆ and Cr(CO)₅ are also determined at the MCPF, CCSD and CCSD(T) levels of theory. The CCSD(T) method gives a much larger total binding energy than either the MCPF or CCSD methods. An analysis of the basis set superposition error (BSSE) at the MCPF level of treatment points out limitations in the one-particle basis used here and in a previous study. Calculations using larger basis sets reduce the BSSE, but the total binding energy of Cr(CO)₆ is still significantly smaller than the experimental value, although the first CO bond dissociation energy of Cr(CO)₆ is well described. An investigation of 3s3p correlation reveals only a small effect. The remaining discrepancy between the experimental and theoretical total binding energy of Cr(CO)₆ is probably due to limitations in the one-particle basis, rather than limitations in the correlation treatment. In particular an additional *d* function and an *f* function on each C and O are needed to obtain quantitative results. This is underscored by the fact that

even using a very large primitive set (1042 primitive functions contracted to 300 basis functions), the superposition error for the total binding energy of Cr(CO)₆ is 22 kcal/mol at the MCPF level of treatment.

- “The fraternal twins of quartet O₄⁺”, R. Lindh and L. A. Barnes, J. Chem. Phys., **100**, 224–237, (1994)

Eleven stationary geometries of quartet O₄⁺ have been studied by *ab initio* methods. The geometries were optimized at the CASSCF level of theory and the energies were calculated by the CASPT2 method, using DZP, TZ2P, ANO[5s4p2d] and ANO[6s5p3d2f] basis sets. The rectangular and *trans*-planar structures are found to be the most stable, with an energy barrier to conversion between the two at the threshold of dissociation. Both have a delocalized hole and are stable relative to separated O₂ and O₂⁺ by 11.0 and 11.5 kcal/mol for the rectangular and the *trans*-planar structure, respectively, compared with the experimentally deduced energy in the range of 9.2 to 10.8 kcal/mol. The adiabatic ionization potentials of O₄ and O₂ are computed to be 11.67 and 12.21 eV, while experimental values are 11.66 and 12.07 eV, respectively. The vibrational frequencies have been computed for all degrees of freedom at the CASSCF level of theory. Symmetry breaking is found to be a particular problem in the computation of the antisymmetric stretch frequency for the delocalized structures at the CASSCF level of theory. Attempts to

rectify these problems using the RASSCF method leads to additional difficulties, but further analysis yields insight into the symmetry breaking and problems with earlier calculations. Finally, a non-orthogonal CI calculation based on the interaction of localized CASSCF wavefunctions using the CASSI method leads to a balanced treatment of the antisymmetric stretch which is free from symmetry breaking. The study explains the four most prominent absorption frequencies observed in the partially unassigned IR spectrum of O_4^+ isolated in solid neon as the antisymmetric OO-stretch, and the combination band of the symmetric and antisymmetric OO-stretch of *both* the rectangular and *trans*-planar structures.

- “Symmetry Breaking in O_4^+ : an application of the Brueckner Coupled Cluster Method”, L. A. Barnes and R. Lindh, Chem. Phys. Lett., **223**, 207, (1994)

A recent calculation of the antisymmetric stretch frequency for the rectangular structure of quartet O_4^+ using the QCISD(T) method gave a value of 3710 cm^{-1} . This anomalous frequency is shown to be a consequence of symmetry breaking effects, which occur even though the QCISD(T) solution derived from a delocalized SCF reference function lies energetically well below the two localized (symmetry-broken) solutions at the equilibrium geometry.

The symmetry breaking is *almost* eliminated at the CCSD level of theory, but the small remaining symmetry breaking effects are magnified at the CCSD(T)

level of theory so that the antisymmetric stretch frequency is still significantly in error. The use Brueckner coupled cluster method, however, leads to a symmetrical solution which is free of symmetry breaking effects, with an antisymmetric stretch frequency of 1322 cm^{-1} , in good agreement with our earlier calculations using the CASSCF/CASSI method.

- “A multi-region integration scheme”, L. A. Barnes, work in progress (to be published)

In this preliminary report, a multi-region radial integration is compared to the recently proposed method due to Handy *et al.*. Preliminary results for small systems indicate that the new integration scheme is generally comparable to and sometimes better than that of Handy *et al.*, although this conclusion is by no means firm. Work for larger systems is continuing.

Symmetry breaking in O₄⁺: an application of the Brueckner coupled-cluster method

Leslie A. Barnes*

Eloret Institute

Palo Alto, CA 94303, USA

and

Roland Lindh

Dept. of Theoretical Chemistry

University of Lund

Chemical Centre

P. O. Box 124

S-221 00 Lund, Sweden

Abstract

A recent calculation of the antisymmetric stretch frequency for the rectangular structure of quartet O₄⁺ using the QCISD(T) method gave a value of 3710 cm⁻¹. This anomalous frequency is shown to be a consequence of symmetry breaking effects, which occur even though the QCISD(T) solution derived from a delocalized SCF reference function lies energetically well below the two localized (symmetry-broken) solutions at the equilibrium geometry. The symmetry breaking is *almost* eliminated at the CCSD level of theory, but the small remaining symmetry breaking effects are magnified at the CCSD(T) level of theory so that the antisymmetric stretch frequency is still significantly in error. The use Brueckner coupled cluster method, however, leads to a symmetrical solution which is free of symmetry breaking effects, with an antisymmetric stretch frequency of 1322 cm⁻¹, in good agreement with our earlier calculations using the CASSCF/CASSI method.

* Mailing address: NASA Ames Research Center, Moffett Field, California 94035-1000

Introduction

Recently, Peel [1] reported *ab initio* calculations on some high symmetry isomers of quartet O_4^+ using the singles and doubles quadratic configuration interaction method with a perturbational estimate of connected triple excitations (QCISD(T)) [2]. For the rectangular structure, he obtained an antisymmetric stretch frequency of 3710 cm^{-1} , which he noted was “unphysical”, but nevertheless was used to give a large zero-point correction to the energy of this isomer.

Previously [3], we had carried out a detailed study of several structures of quartet O_4^+ , computing amongst other things vibrational frequencies, relative energies and isotopic shifts. The methods used included complete active space self consistent field (CASSCF) [4], restricted active space self consistent field (RASSCF) [5], a second order perturbation method based on a CASSCF reference function (CASPT2) [6] and a non-orthogonal CI method based on non-orthogonal CASSCF or RASSCF solutions (the complete/restricted active space state interaction (CASSI/RASSI) method [7]), using large generally contracted atomic natural orbital basis sets. These methods gave good results and prompted a new analysis [8] of the experimental vibrational spectrum of O_4^+ , which supported our assignment. Of particular importance for the current work is our detailed analysis of symmetry breaking effects in the calculation of the antisymmetric stretch frequency for quartet O_4^+ . We showed that spurious frequencies for quartet O_4^+ were due to symmetry breaking effects due to the competition between localized and delocalized structures — we refer the reader to our original work [3], where we also give many references to earlier work on symmetry breaking. In our case, the symmetry breaking effects were resolved through the use of the CASSI method, allowing the two non-orthogonal “localized” CASSCF wavefunctions to interact and give the correct qualitative form for the potential energy surface.

On the basis of the form of the potential curve for the antisymmetric stretch around the equilibrium point for the rectangular structure, Peel [1] concluded that no symmetry breaking effects were evident at the QCISD(T) level of theory. In the first part of this work we demonstrate that this is incorrect: symmetry breaking effects are entirely responsible for the anomalous antisymmetric stretch frequency of 3710 cm^{-1} . For consistency, we use the same methods as in Ref. [1] — QCISD(T) calculations based on an unrestricted Hartree Fock (UHF) reference function and a 6-31G* basis set. The geometry ($R_{OO}=1.186\text{ \AA}$, $R_{CM}=2.378\text{ \AA}$) was also taken from Ref. [1]. R_{OO} is the intra-fragment O–O bond distance, R_{CM} is the inter-fragment bond distance (the distance between the center of masses of the two fragments). The rectangular structure is illustrated in Fig. 1(a), which also shows R_{OO} and R_{CM} .

Following this, we give the results of calculations at the CCSD(T) level of theory (singles and doubles coupled-cluster plus a perturbational estimate of the effects of connected triples excitations [9]). The geometry is reoptimized and from the computed potential curves and frequencies it is evident that symmetry breaking effects also occur at the CCSD(T) level of theory. Brueckner coupled cluster theory [10]–[15] has previously been used to treat symmetry breaking effects at the coupled cluster level of theory [16]. We

have applied this approach to the rectangular structure of quartet O_4^+ , using Brueckner coupled cluster calculations which include a perturbational estimate of the effects of connected triples excitations (BD(T)) [14], with semi-canonical orbitals [17]. Since we are interested in the qualitative nature of the results, rather than strictly quantitative results, we continue to use the 6-31G* basis set and UHF reference function, rather than the larger generally contracted basis sets of our earlier study [3]. We note that in the CCSD(T) and BD(T) calculations, all electrons are correlated, whereas in the QCISD and QCISD(T) calculations, the $1s$ core electrons were not correlated.

The calculations were performed with the ACES II¹ suite of programs using IBM RISC SYSTEM/6000 computers at NASA Ames Research Center.

Results and Discussion

As discussed in detail in our previous work [3], the symmetry breaking in O_4^+ is manifested by the existence of a delocalized solution, which exhibits D_{2h} symmetry, and two localized solutions exhibiting C_{2v} symmetry which are mirror images of each other, having equal energies at the symmetric (D_{2h}) point. The structures are illustrated in Fig. 1, with Fig. 1(a) showing the symmetric geometry, and Figs. 1(b) and (c) showing the two symmetry broken localized solutions. In each case, the shorter O–O bond distance corresponds closely to the bond distance of O_2^+ , whereas the longer bond distance corresponds closely to the bond distance of O_2 [3]. Thus the positive charge is localized on the bottom O_2 unit in Fig. 1(b), and on the top O_2 unit in Fig. 1(c). The symmetry breaking vibrational mode is the intra-fragment antisymmetric stretch ω_5 , and this is illustrated in Figs. 1(b) and (c) by the arrows.

In Table I, we give the total energies of the different solutions at the UHF, QCISD and QCISD(T) levels of theory. Comparing the total energy at the QCISD(T) level with that given in Ref. [1], we see that the results of Ref. [1] are based on the delocalized reference function. It is interesting to compare the energy differences of the delocalized and localized solutions at the various levels of theory. At the UHF and QCISD levels of theory, the localized solution is *below* the delocalized solution by about 3 kcal/mol. However, at the QCISD(T) level of theory, the localized solution is more than 7 kcal/mol *higher* in energy than the delocalized solution. Thus it seems that the D_{2h} structure is favoured at the highest level of theory.

To understand the origin of the spurious frequency at the QCISD(T) level of theory, we have computed the energy as a function of the antisymmetric stretch coordinate (see

¹ACES II is a computational chemistry package especially designed for coupled cluster and many body perturbation calculations. The SCF, transformation, correlation energy and gradient codes were written by J. F. Stanton, J. Gauss, J. D. Watts, W. J. Lauderdale and R. J. Bartlett. The two-electron integrals are taken from the vectorized MOLECULE code of J. Almlöf and P. R. Taylor. ACES II includes a modified version of the ABACUS integral derivatives program, written by T. Helgaker, H. J. Jensen, P. Jørgensen, J. Olsen, and P. R. Taylor, and the geometry optimization and vibrational analysis package written by J. F. Stanton and D. E. Bernholdt.

also Refs. [1] and [3]). The results are presented in Figs. 2–4, where we have used the same scales in order to facilitate comparison of the different curvatures resulting from the different methods. The delocalized solution is given by E_{del} and the two localized solutions are given by E_a and E_b in each case. Also given in Figs. 3 and 4 are curves at the CCSD, CCSD(T), BD and BD(T) level of theory, which we discuss later. Using the notation of Figs. 1(b) and (c), ΔR is defined as $R_1 - R_2$.

The behaviour of the energy at the correlated level of theory is driven by the behaviour of the UHF energies, given in Fig. 2. The delocalized solution lies above the localized solutions, and as we follow the antisymmetric coordinate, the delocalized solution rapidly approaches the localized solutions, until at $\Delta R \approx 0.0185$ Å the localized and delocalized solutions merge. Thus the QCISD and QCISD(T) energies are constrained by this fact — the delocalized energy and one of the localized energies (depending on whether the distortion is positive or negative) must be equal at $\Delta R \approx 0.0185$ Å. In Fig. 3, we see that at the QCISD level of theory the energies are significantly better in the sense that the localized solution energies are much flatter (tending towards delocalized solutions). In this case the flatness of the localized solutions means that the delocalized solution is driven *down* in energy in order to meet the constraint of equal energy at $\Delta R \approx 0.0185$ Å, leading to an imaginary frequency at the QCISD level of theory. At the QCISD(T) level of theory (Fig. 4) the delocalized solution is well below the localized solution, and so is driven *rapidly upward* to meet the equal energy constraint, resulting in the very large 3710 cm^{-1} frequency. Thus the QCISD method does not entirely overcome the inherent problems with the UHF reference function, and the triples perturbation correction is unable to overcome the residual problems with the QCISD method. We note that we found similar problems with the CASPT2 method, which was not able to overcome the problems of a localized CASSCF reference function [3].

In Tables II and III we present the results from the CCSD(T) calculations. From the energy separations, we see that while the UHF separation is very similar to that given in Table I (which has a slightly different geometry), the CCSD and CCSD(T) separations are very different to those at the QCISD and QCISD(T) levels of theory. The delocalized and localized solutions are very close in energy at the CCSD level of theory, and unlike the QCISD results the localized solution is above the delocalized solution. As for the QCISD(T) results, the perturbational triples correction increases the separation between the delocalized and localized solutions at the CCSD(T) theory when compared with CCSD, although the effect is much smaller than the QCISD and QCISD(T) difference. We note that one difference between the QCISD and CCSD calculations was that the 1s core electrons were excluded from the calculations at the QCISD and QCISD(T) levels of theory, whereas they were included in the calculations at the CCSD and CCSD(T) levels of theory. To check whether this difference has any effect on the symmetry breaking at the QCISD/QCISD(T) level of theory, we also computed the separation between the delocalized and localized solutions at the symmetric point including the 1s electrons using these methods. The separations are barely different from the original results, so we conclude that removing the core 1s electrons from the QCISD calculations is not the cause of the large difference between the CCSD/CCSD(T) and QCISD/QCISD(T) results.

In Figs. 3 and 4 we present the CCSD and CCSD(T) potential curves for the antisymmetric

stretch, which may be compared with the QCISD and QCISD(T) curves on the same figures. The behaviour of the UHF reference function energies around the CCSD(T) equilibrium geometry for the antisymmetric stretch is very similar to that given in Fig. 2 around the QCISD(T) equilibrium geometry, so we may discuss the CCSD and CCSD(T) curves in the same light as the QCISD and QCISD(T) curves. Thus the CCSD and CCSD(T) energies have similar constraints to the QCISD and QCISD(T) energies — irrespective of the separation at $\Delta R=0$ (the symmetric geometry), at $\Delta R \approx 0.0185\text{\AA}$ the delocalized and one of the localized energies must be equal. Inspection of the curves shows that this is so. However, the most striking difference between the CCSD and QCISD curves comes from the fact that the curves at the CCSD level are much closer together, so that this constraint has only a small effect on the antisymmetric stretch frequency at the CCSD level of theory. In fact, the antisymmetric stretch frequency at the CCSD level of theory is a very reasonable 1220 cm^{-1} (at the CCSD equilibrium geometry), which is to be compared with a value of around 1500 cm^{-1} at the QCISD level of theory. Overall, we see that the CCSD approach has *almost* eliminated the symmetry breaking effects.

As discussed above, the addition of the perturbative triples correction increases the separation between the delocalized and localized solutions at the symmetric point, and this is evident in Fig. 4. Thus the delocalized curve at the CCSD(T) level is more affected by symmetry breaking than the CCSD curve, although this effect is much smaller than that found with the QCISD(T) method. Thus the antisymmetric stretch frequency at the CCSD(T) level is 1922 cm^{-1} , compared with 3710 cm^{-1} at the QCISD(T) level of theory. The origin of this difference is quite evident from the potential curves — it is the large difference in separations at the symmetric point. The other remarkable feature of the CCSD(T) potential curves is the near coincidence of the two localized curves, which is again quite different to the QCISD(T) results. Thus the CCSD(T) approach is quite close to removing the symmetry breaking effects, but is still not able to overcome the small deficiencies evident at the CCSD level of theory.

The geometry at the CCSD(T) level (Table III) is very similar to that found at the QCISD(T) level of theory [1], and for the most part the frequencies are quite similar to those given in Ref. [1]. The exceptions are the antisymmetric stretch ω_5 (discussed above) which changes from 3710 to 1922 cm^{-1} , and the (inter-fragment) antisymmetric stretch ω_6 which is reduced from 595 to 97 cm^{-1} . The CCSD(T) value for ω_6 is in accord with our earlier results [3] and the results for the *trans*-planar structure [1, 3]. Thus it seems that the QCISD(T) value for ω_6 is significantly too high also. Considering Fig. 1, the mode ω_6 may be envisioned in an analogous way to ω_5 , except that the distortion occurs along the R_{CM} direction instead of the R_{OO} direction. Thus it is possible, though less likely (due to the large inter-fragment bond distance R_{CM}), for symmetry breaking effects to occur for ω_6 also. This would involve localization on the left and right sides of O_4^+ rather than the top and bottom, which occurs for ω_5 . However, we have not investigated this in any detail here.

The results at the BD(T) level of theory are given in Table IV. The geometry optimized at the BD(T) level of theory is the same as that of the CCSD(T) level of theory (which was constrained to have D_{2h} symmetry, whereas the BD(T) calculation was not), and the BD(T) energy is also very similar to the CCSD(T) energy. To investigate whether

symmetry breaking effects are still present at the BD(T) level of theory, we have again plotted the energy as a function of the antisymmetric distortion, and the results are given in Figs. 3–5.

As we saw previously, the behaviour of the correlated methods was constrained by the behaviour of the reference function. In Fig. 5 we give the Brueckner reference determinant energy and the UHF energy from which the Brueckner calculation was initiated. Before discussing these results, we emphasize that the comparison between the Brueckner reference determinant energy and the UHF energy is not rigorous since the Brueckner reference determinant is a *product* of the correlated calculation. Nevertheless, it is enlightening.

The UHF solutions of Fig. 5 are (qualitatively speaking) a subset of those given in Fig. 2. The curve is discontinuous because we varied ΔR with a larger stepsize than for Fig. 2, and the SCF converged to solutions on different potential curves at different points, rather than the solution on the same potential curve as in Fig. 2. The character of the UHF orbitals is of course very different for the different potential energy surfaces, varying from delocalized to localized on the top of the molecule or localized on the bottom of the molecule, and this variation is reflected in the energies. In contrast to this, the Brueckner reference energy is very smooth despite the large changes in the UHF orbitals from which it began, indicating that the Brueckner approach is not affected by the starting orbitals. At the symmetric point we have also verified that the Brueckner method is independent of the starting orbitals — whether localized or delocalized UHF orbitals are used, the Brueckner approach leads to the same symmetric (delocalized) solution. Thus there is *only one* solution at the Brueckner level of theory. This behaviour is in accord with previous studies [16] using the Brueckner approach for other systems which exhibit symmetry breaking.

At the BD and BD(T) levels of theory (Figs. 3 and 4) we see that the antisymmetric stretch is very smooth and gives a positive frequency, which is 1322 cm^{-1} at the BD(T) level of theory (Table IV). It is interesting to compare the different curvatures for the different methods in Figs. 3 and 4. It is evident that the CCSD and CCSD(T) curvatures are much closer to the BD and BD(T) curves than are those from QCISD and QCISD(T).

We note from our previous study [3] that there is a significant basis set effect for the antisymmetric stretch frequency. At the CASSI level using a TZ2P basis set, the antisymmetric stretch was 1271 cm^{-1} whereas an ANO[5s4p2d] basis set gave a value of 1259 cm^{-1} and an ANO[6s5p3d2f] basis gave a value of 1296 cm^{-1} . Considering the fact that the BD(T) approach should give a larger proportion of the dynamical correlation energy than our earlier frequency calculations at the CASSCF/CASSI level of theory, the agreement between the BD(T) frequency and our earlier values is very good. Thus the BD(T) results are very encouraging and in a large one particle basis this method should give very accurate results. In our earlier work [3] we showed that the dipole derivative at the CASSI level of theory was unphysically high. It would be of some interest to compute this quantity at the BD(T) level (in a large one particle basis) to determine whether a more reasonable dipole derivative would be obtained.

In Table IV we also give the symmetric stretch frequencies at the BD(T) level of theory.

Given the agreement between the geometries at the CCSD(T) and BD(T) levels of theory, it is not surprising that the symmetric stretch frequencies are very similar for the two methods (and also in good agreement with the CASSCF results [3]). These results also support our earlier isotopic substitution analysis [3], where we used the CASSCF frequency for the symmetric stretch and the CASSI frequency for the antisymmetric stretch.

To conclude, the antisymmetric stretch of quartet O_4^+ is significantly affected by symmetry breaking. As we discussed previously [3], it is necessary to properly account for this before a reliable frequency can be obtained. In the current work we have shown in detail how the previous [1] antisymmetric stretch frequency at the QCISD(T) level of theory is affected by symmetry breaking so that any analysis of the relative energies of the rectangular and trans-planar structures which includes zero-point corrections based on this frequency must be significantly in error. The CCSD approach gives significantly better results than QCISD, *almost* eliminating the symmetry breaking effects. However, the small remaining symmetry breaking effects are magnified at the CCSD(T) level of theory, so that the antisymmetric stretch is still affected significantly at the CCSD(T) level. The Brueckner coupled-cluster method (BD(T)), however, eliminates the symmetry breaking effects entirely, giving a single symmetric solution with an antisymmetric stretch frequency in good agreement with our earlier result at the CASSCF/CASSI level of theory [3]. This must make the BD(T) approach the method of choice for very accurate calculations when symmetry breaking is a potential problem and more than just a few electrons must be correlated.

Acknowledgements

L.A.B. was supported by NASA grant number NCC-2-741, and R.L. was supported by a grant from the Swedish Natural Research Council (NFR) and by IBM Sweden under a joint study contract. The receipt of a preprint of Ref. [1] is acknowledged.

References

- [1] J. B. Peel, *Chem. Phys. Lett.* **218**, 367 (1994).
- [2] J. A. Pople, M. Head-Gordon, and K. Raghavachari, *J. Chem. Phys.* **87**, 5968 (1987).
- [3] R. Lindh and L. A. Barnes, *J. Chem. Phys.* **100**, 224 (1994).
- [4] P.-Å. Malmqvist, A. Rendell, and B. O. Roos, *J. Chem. Phys.* **94**, 5477 (1990), and references therein.
- [5] J. Olsen, B. O. Roos, P. Jørgensen, and H. J. Aa. Jensen *J. Chem. Phys.* **89**, 2185 (1985).
- [6] K. Andersson, P.-Å. Malmqvist, B. O. Roos, A. J. Sadlej, and K. Wolinski, *J. Chem. Phys.* **94**, 5483 (1990); K. Andersson, P.-Å. Malmqvist, and B. O. Roos, *ibid* **96**, 1218 (1992).
- [7] P.-Å. Malmqvist , *Int. J. Quant. Chem.* **30**, 479 (1986); P.-Å. Malmqvist and B. O. Roos, *Chem. Phys. Lett.* **155**, 189 (1989).
- [8] M. E. Jacox and W. E. Thompson, *J. Chem. Phys.* **100**, 750 (1994).
- [9] K. Raghavachari, G. W. Trucks, J. A. Pople, and M. Head-Gordon *Chem. Phys. Lett.* **157**, 479 (1989).
- [10] K. A. Brueckner, *Phys. Rev.* **96**, 508 (1954).
- [11] R. K. Nesbet, *Phys. Rev.* **109**, 1632 (1958).
- [12] R. A. Chiles and C. E. Dykstra, *J. Chem. Phys.*, **74**, 4544 (1981).
- [13] L. Z. Stolarczyk and H. J. Monkhorst, *Int. J. Quantum Chem. Symp.* **18**, 267 (1984).
- [14] N. C. Handy, J. A. Pople, M. Head-Gordon, K. Raghavachari, and G. W. Trucks *Chem. Phys. Lett.* **164**, 185 (1989).
- [15] K. Raghavachari, J. A. Pople, E. S. Replogle, M. Head-Gordon, and N. C. Handy, *Chem. Phys. Lett.* **167**, 115 (1990).
- [16] J. F. Stanton, J. Gauss, and R. J. Bartlett, *J. Chem. Phys.* **97**, 5554 (1992).
- [17] J. D. Watts, J. Gauss, and R. J. Bartlett, *J. Chem. Phys.* **98**, 8718 (1993).

Table I: Total energies (in Hartree) and energy differences (in kcal/mol) of quartet O_4^+ at the rectangular (D_{2h}) geometry, for the delocalized and localized solutions. The geometry is taken from the QCISD(T) calculations of Ref.[1] ($R_{OO}=1.186$ Å, $R_{CM}=2.378$ Å)

Method	E_{del}	E_{loc}	ΔE
UHF	-298.7398444	-298.7439668	2.59
QCISD	-299.4774306	-299.4830304	3.51
QCISD(T)	-299.5050169	-299.4933392	-7.33

Table II: Total energies (in Hartree) and energy differences (in kcal/mol) of quartet O_4^+ at the rectangular (D_{2h}) geometry, for the delocalized and localized solutions. The geometry is from the CCSD(T) approach, given in Table III

Method	E_{del}	E_{loc}	ΔE
UHF	-298.7406630	-298.7447092	2.54
CCSD	-299.4838322	-299.4832236	-0.38
CCSD(T)	-299.5127862	-299.5107674	-1.27

Table III: Total energy (in Hartree), geometrical parameters (in Å) and frequencies (in cm^{-1}) of quartet O_4^+ at the rectangular (D_{2h}) geometry, using the CCSD(T) approach.

E	-299.5127862
R_{OO}	1.1846
R_{CM}	2.3751
$\omega_1(a_g)$	1713
$\omega_2(a_g)$	271
$\omega_3(b_{1g})$	372
$\omega_4(a_u)$	175
$\omega_5(b_{3u})$	1922 ^a
$\omega_6(b_{2u})$	97

^a This frequency was computed as a finite difference of energies, since the symmetry breaking effects lead to spurious results from the automatic finite difference of gradients approach of Aces II (which used different UHF solutions at different points of the finite difference procedure). However, the automated approach was used for the other frequencies, including ω_6 (which was also computed by finite difference of energies as a check).

Table IV: Total energy (in Hartree), geometrical parameters (in Å) and frequencies (in cm^{-1}) of quartet O_4^+ at the rectangular (D_{2h}) geometry, using the BD(T) approach.

E	-299.5127780
R_{OO}	1.1846
R_{CM}	2.3751
$\omega_1(a_g)$	1713
$\omega_2(a_g)$	270
$\omega_5(b_{3u})$	1322

Figure captions

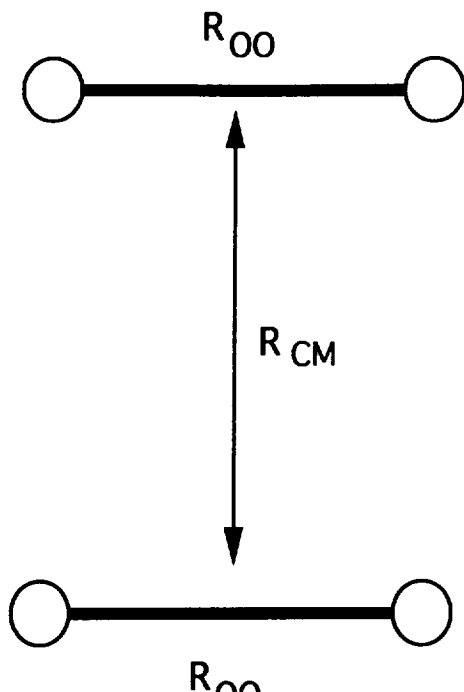
Figure 1: Schematic structures of rectangular O_4^+ . (a) The symmetric structure (D_{2h} symmetry). (b) The bottom localized structure (C_{2v} symmetry). (c) The top localized structure (C_{2v} symmetry). The antisymmetric stretch mode ω_5 is illustrated schematically with arrows.

Figure 2: UHF energies (around the QCISD(T) equilibrium geometry) as a function of the antisymmetric stretch coordinate for the rectangular structure of O_4^+ . E_a is given by \diamond , E_b is given by $+$ and E_{del} is given by \square .

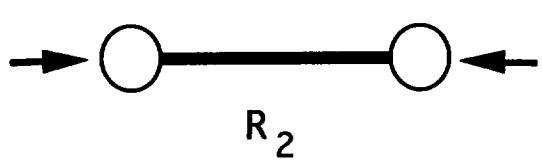
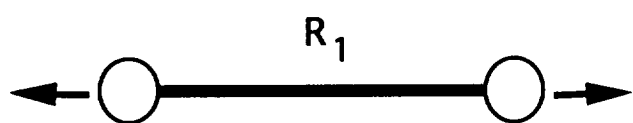
Figure 3: QCISD, CCSD and BD energies (around the QCISD(T), CCSD(T) and BD(T) equilibrium geometries, respectively) as a function of the antisymmetric stretch coordinate for the rectangular structure of O_4^+ . The QCISD energies E_a are given by \diamond , E_b are given by $+$ and E_{del} are given by \square . The analogous CCSD energies are given by \times , Δ and \star , respectively. The BD energies are given by \bullet . For clarity, the CCSD energies are offset by -0.005 Hartree, whereas the BD energies are offset by -0.01 Hartree.

Figure 4: QCISD(T), CCSD(T) and BD(T) energies as a function of the antisymmetric stretch coordinate for the rectangular structure of O_4^+ . The QCISD(T) energies E_a are given by \diamond , E_b are given by $+$ and E_{del} are given by \square . The analogous CCSD(T) energies are given by \times , Δ and \star , respectively. The BD(T) energies are given by \bullet . For clarity, the CCSD(T) energies are offset by 0.0025 Hartree.

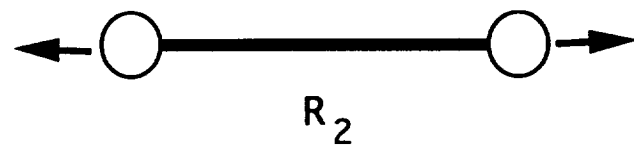
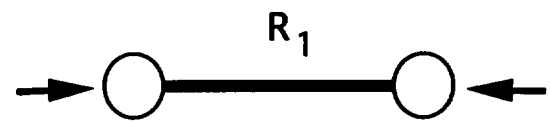
Figure 5: UHF and Brueckner determinant reference energies as a function of the antisymmetric stretch coordinate for the rectangular structure of O_4^+ . The UHF energies are given by \diamond and the Brueckner determinant reference energy is given by $+$



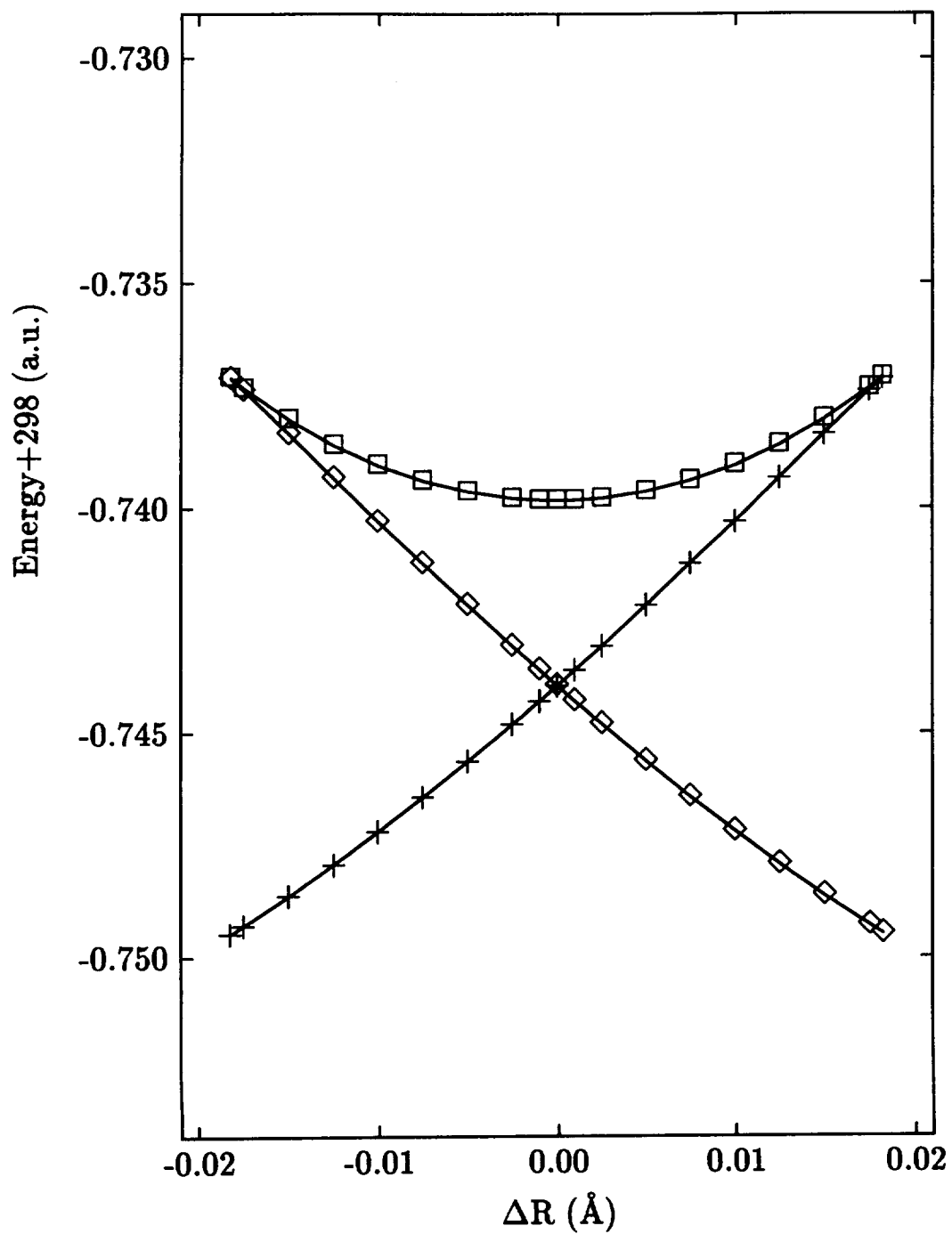
(a)

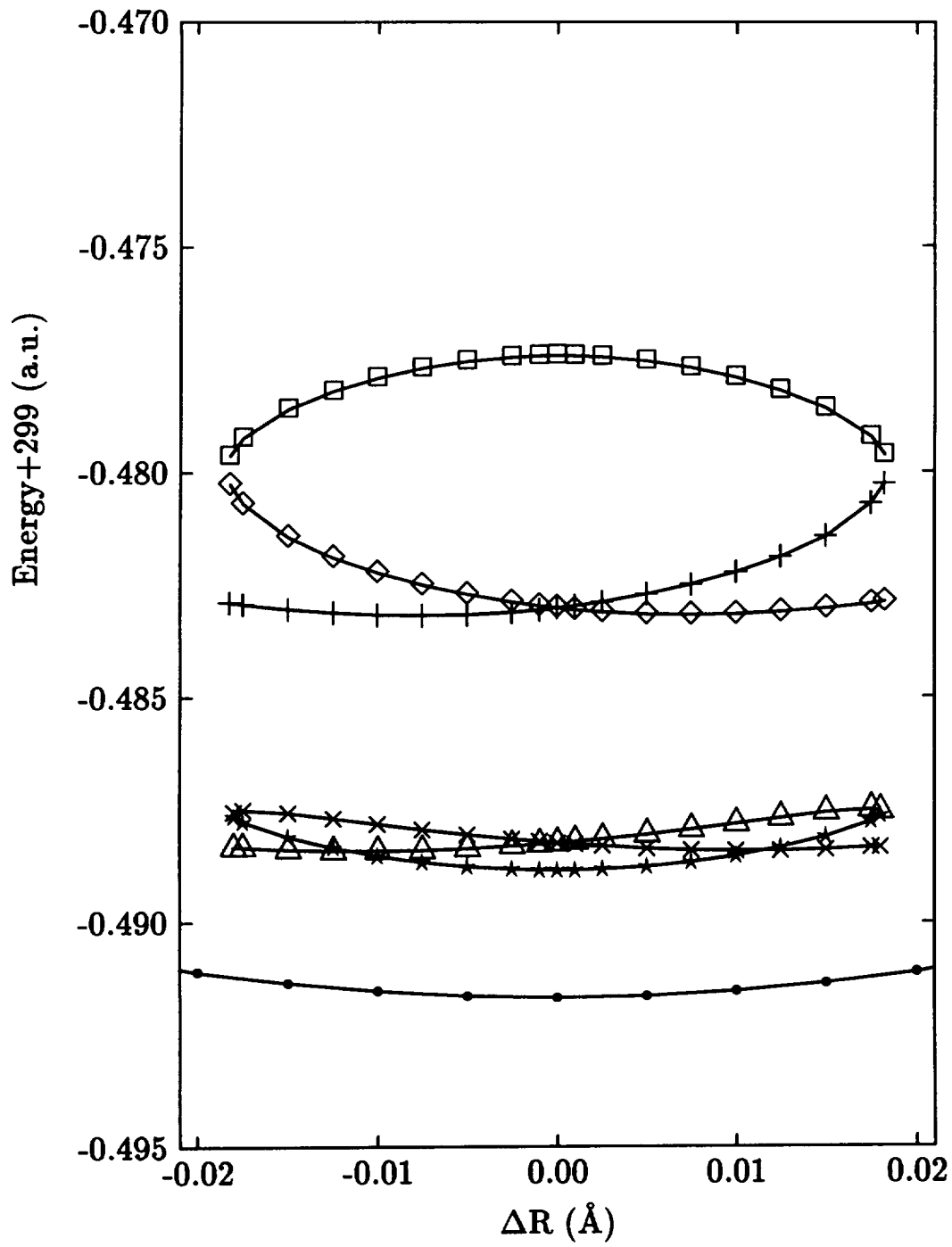


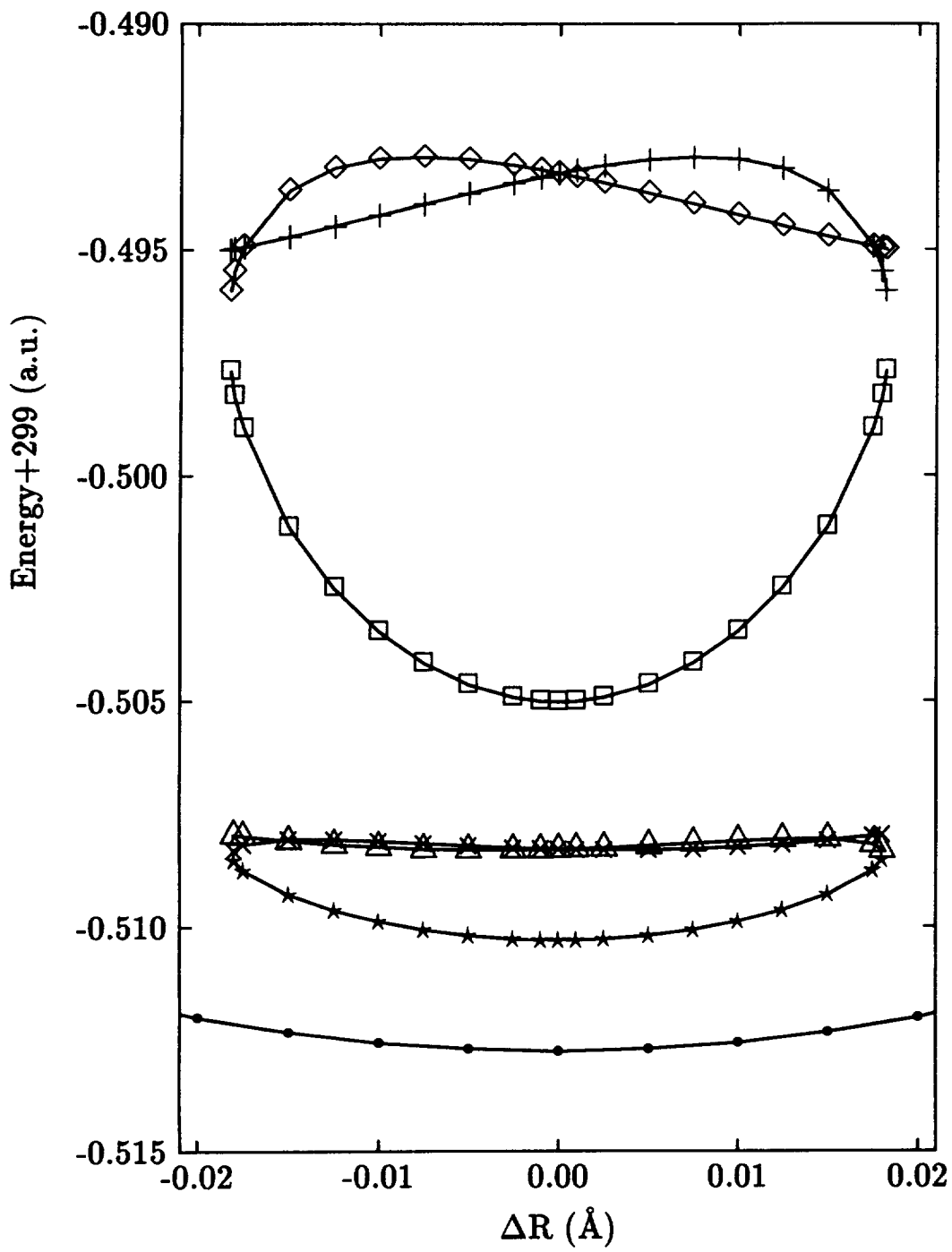
(b)

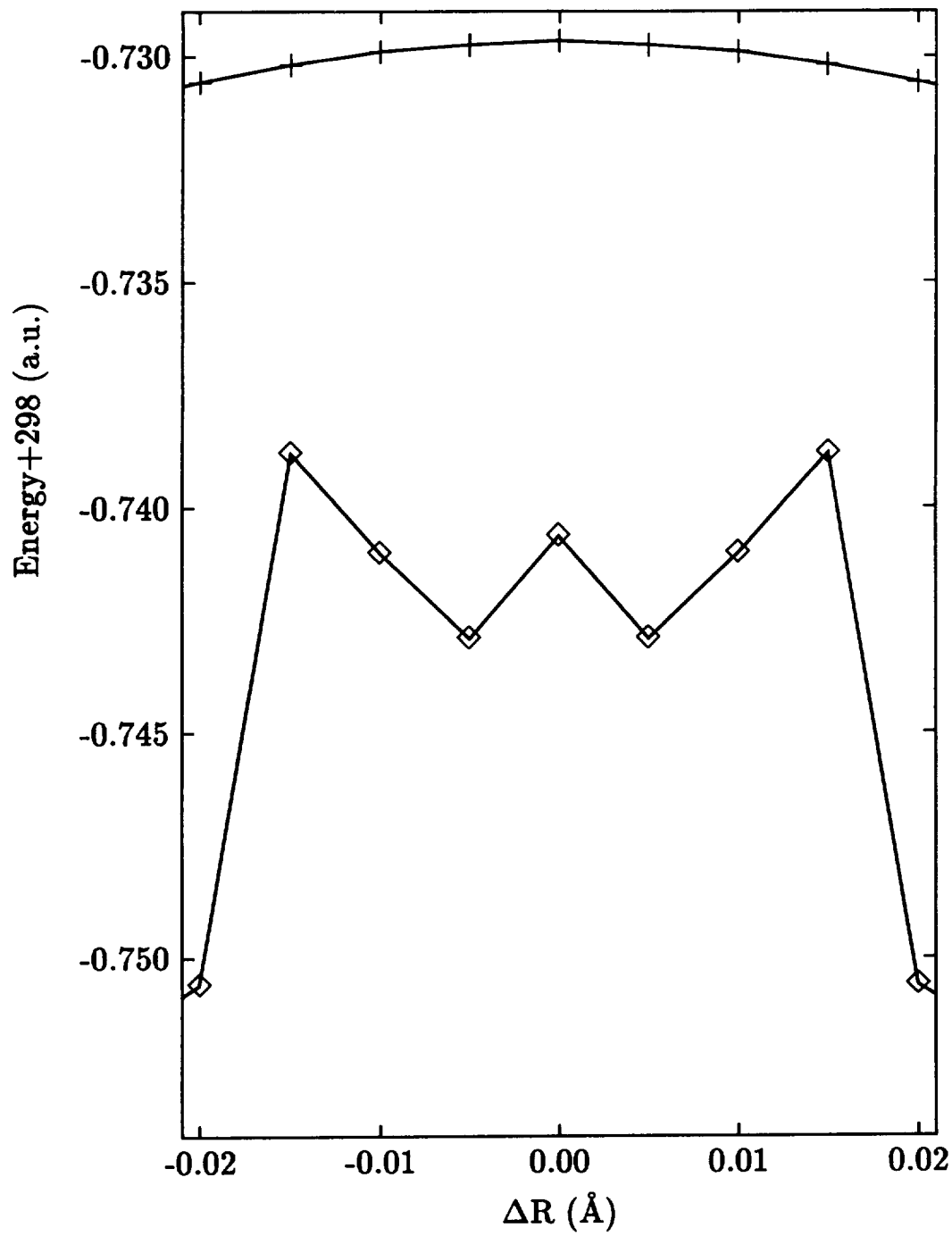


(c)









A multi-region radial integration scheme

Leslie A. Barnes *

Eloret Institute

Palo Alto

California 94303

Abstract

In this preliminary report, a multi-region radial integration is compared to the recently proposed method due to Handy *et al.*. Preliminary results for small systems indicate that the new integration scheme is generally comparable to and sometimes better than that of Handy *et al.*, although this conclusion is by no means firm. Work for larger systems is continuing.

*Mailing Address: NASA Ames Research Center, Moffett Field, California 94035-1000

1 Introduction

There is recently a great deal of interest in the testing and application of Density Functional techniques for use in molecular calculations. The complicated functional forms used in this theory preclude analytical integration, so that numerical methods must be used. Recently, Handy *et al.*[1] proposed a radial integration based on the Euler-Maclaurin summation giving good results for a number of systems. However, it is worthwhile investigating other methods since for accurate calculations many quadrature points are required in general, even with the Euler-Maclaurin technique. In addition, one problem with the Euler-Maclaurin scheme is that there is little control over the location of additional quadrature points. For example, this scheme is very efficient for atoms, but in a molecular context additional points are required for an integration which is comparable to the atomic case. These additional points should ideally be placed in the valence region. However, with the Euler-Maclaurin scheme points must be placed throughout the entire region. This problem is bypassed with a multiregion integration.

The advantage of the multiregion integration is the control of the placement of additional quadrature points in the molecular situation. In general, we determine an accurate quadrature for the constituent atoms or small molecular fragments. In the molecular situation we then only need to add points to the valence region(s), and increase the accuracy of the angular quadrature, in order to be able to produce an accurate molecular quadrature. One disadvantage of the multiregion integration is a possible increase in errors due to the accumulation of errors from the individual regions.

Here we investigate the efficiency of a multi-region integration similar to that previously proposed by Te Velde and Baerends [2] and also Thakar [3]. One difference in the current work is the use of a change of variables due to McLean and Yoshimine [4] which allows for efficient placement of the quadrature points by mapping the region $[a, m, b]$ onto the region $[-1, 0, 1]$, where a and b are the endpoints of the region, and m is any point between a and b . This mapping takes the form

$$x = c_1 + c_2(1 + \beta)/(1 - \beta t).$$

The constants c_1 , c_2 and β are completely determined by the mapping $a \rightarrow -1$, $m \rightarrow 0$, and $b \rightarrow 1$. This mapping may be used for all ranges except the doubly infinite range $(-\infty, \infty)$, providing appropriate limiting forms are used for special cases.

The regions used here are based on the atomic charge density, in a spirit similar

to that used by Thakar [3]. However, rather than using a general rule based on the atomic number by which to determine the regions, we use the atomic charge density directly. The function $r^2 * \rho(r)$ is generated numerically, and analysed for maxima, minima and points of inflection. In general, the regions we define are based on these points, in particular the points a and b map onto two minima in the charge density, and the point m maps onto the maximum in between these. These three points define a shell, and the mapping ensures an optimal distribution of quadrature points in the region. Generally we have one region for each shell, with the valence shell being split into an inner and outer parts at the point of inflection of the valence shell (see also Thakar), and the innermost (core) region into two at the first point of inflection. Although this scheme may seem somewhat complicated, in fact it is straightforward to generate the required regions and tabulate them for any atom.

For the inner regions we use a standard Gauss-Legendre quadrature, whereas for the outer region we use a shifted Gauss-Laguerre scheme based on the weight function $e^{-\alpha r}$, where α is related to the highest occupied MO eigenvalue (or the IP) by $\alpha = 2(\sqrt{-2\epsilon_i})$ (see also Thakar [3]).

The other details of the integration are very similar to that proposed by Handy *et al.* [1]. We use a product scheme for the angular integration identical to that of Handy *et al.*, including the use of the angular crowding parameter K_θ . The single center integration scheme of Becke [5] is used, but we use the cutoff function due to Handy *et al.*, with standard Bragg-Slater radii.

We consider three systems here - Ne, Cu and CO. We compare the Euler-Maclaurin to the current multiregion integration for all four systems. We consider integration of the total charge density only here, at the SCF level of approximation, since Handy *et al.* [1] showed that this gives a good indication of the overall performance of an integration scheme. For Ne, we use the Dunning [6] [5s4p] contracted Gaussian basis set. For carbon and oxygen we use the correlation consistent polarized valence triple zeta (cc-pVTZ) basis sets of Dunning. For Cu we use a (20s 15p 10d 6f 4g)/[6 + 1s 5 + 1p 4d 2f 1g] basis set derived from the large primitive set of Partridge [7], contracted by Bauschlicher using the atomic natural orbital (ANO) approach. The C-O bond length is 2.2 a.u. in all cases.

The calculations were carried out using the Seward integral program and the Sweden SCF program on the Cray YMP-C90 at NASA Ames research center.

2 Results and Discussion

For Ne atom, the results for the Euler-Maclaurin integration are given in Table 1. We give the number of points used in the radial integration, the number of points including those discarded due to the radial cutoff (in parentheses), the radial factor m_r (Handy *et al.* [1], Eqn. 6), and the total error in the integrated charge density. Our results for this are very similar to Handy *et al.*, as expected, with a very accurate radial integration attained with 72 radial points. In Table 2, we give the results from the multiregion integration, with the number of points in each region given. In region 5 we also indicate the number of points including those discarded due to the radial cutoff, in parentheses. Overall, more radial points are required for the multi-region integration, although the integration is still accurate. For example, if one used a value for m_r in the Euler-Maclaurin integration which was not optimal, then the results could be worse than for the multi-region integration.

In Table 3, we give the results for the integration of Cu atom in a large ANO basis set, for three different numbers of radial points. One trend to be noted is that a higher m_r value is needed for Cu than Ne as more radial points are added, and more radial points are needed to achieve a similar absolute accuracy. As noted by Handy *et al.* this is because the numerical integration only gives a certain *relative* error rather than absolute error in the integration. We note that for Cu atom ($4s^1$) it is necessary to integrate out a long way (22 a.u.) due to the very diffuse nature of the $4s$ orbital, and that sometimes a higher value of m_r can be necessary than that recommended than Handy *et al.* to obtain optimum results.

The multi-region results of Tables 4 and 5 compare quite well with the Euler-Maclaurin results, although again it seems that more points are necessary for the multi-region scheme, depending on the m_r value used for in the Euler-Maclaurin scheme. We note that the inner regions for the multi-region scheme are very compact, due to the higher atomic number in this case, and that quite a few radial points are necessary to describe the density accurately in this compact region. However, this does not necessarily translate to a lot of points in a molecular calculation, since the number of angular points needed in the inner regions is much smaller than in the valence regions.

Finally we consider the CO molecule (Tables 6–8). We use the same number of angular points in for the Euler-Maclaurin and the multi-region integrations ($n_\theta=42$, $n_\phi=84$), and the same Bragg-Slater radii in each case ($r_C=1.32281$ a.u., $r_O=1.13383$ a.u.). Overall, it seems that it is possible for the Euler-Maclaurin scheme

to outperform the multi-radial scheme if the right values of m_r and m_μ (the angular factor [1]) are chosen. However, these differ significantly from the “standard” values recommended by Handy *et al.*, $m_r=2$ or 3 and $m_\mu=10$ or 11. For these values, we see that the multi-region scheme is either equivalent to or better than the Euler-Maclaurin scheme in efficiency. Another interesting point from Tables 6 and 8 is that it is not just the total number of radial points which is important, but also the spread of these points along r , as this affects the total number of points through the angular factors. For example, the spread of radial points in the Euler-Maclaurin scheme is approximately linear on a logarithmic scale, apart from the very short and long range regions. Changing the factor m_r changes the slope of this logarithmic plot, so that for higher values of m_r there are more points in the core region and more points in the long range regions, leading to fewer points overall, since there are fewer angular points in the core region and the long range points are discarded due to the radial cutoff. Thus for the Euler-Maclaurin scheme, very different total numbers of points are realized for $m_r=3$ versus $m_r=4$, even though the nominal number of radial points is the same in each case.

For the multi-region scheme, two sets of results are presented for CO (Table 8), differing in the number of points in the valence and outer regions, and with the total number of points being very comparable to the best results found for the Euler-Maclaurin scheme. One advantage of the multi-region scheme is that we are able to take a set of integration parameters from a similar atom (for example, those for Ne in this case), and then place more radial points in the valence and outer valence regions in order to attain higher accuracy. This can be seen to be an effective way to add points for CO.

Overall, it seems that neither integration scheme is clearly superior in the molecular situation, based on the current results. More and larger systems need to be studied in order to establish whether the multi-region integration scheme proposed here is significantly better to the widely used Euler-Maclaurin scheme of Handy *et al.*[1]

3 Acknowledgements

L.A.B was supported by NASA grant number NCC-2-741. Helpful discussions with D. W. Schwenke, H. Partridge and A. D. McLean are acknowledged. The provision of a subroutine to facilitate the McLean-Yoshimine change of variable by A. D. McLean is acknowledged.

References

- [1] C. W. Murray, N. C. Handy, and G. J. Laming, Mol. Phys. **78**, 997 (1993).
- [2] G. Te Velde and E. J. Baerends, J. Comp. Phys. **99**, 84 (1992).
- [3] A. J. Thakar, Phys. Rev. A **46**, 6920 (1992).
- [4] A. D. McLean and M. Yoshimine, IBM Journal of Research and Development **9**, 203 (1965).
- [5] A. D. Becke, J. Chem. Phys. **88**, 2547 (1988).
- [6] T. H. Dunning, Jr., J. Chem. Phys. **53**, 2823 (1970).
- [7] H. Partridge, J. Chem. Phys. **90**, 1043 (1989).

Table 1: Euler-Maclaurin integration of Ne atom ($r_{max}=15.0$ a.u.)

n_r	m_r	$\Delta\rho(r)$
66(70)	1	3.0×10^{-5}
56(70)	2	3.1×10^{-10}
50(70)	3	8.8×10^{-10}
47(70)	4	7.1×10^{-7}
94(100)	1	6.6×10^{-6}
72(100)	2	9.1×10^{-13}
80(100)	3	3.8×10^{-11}
67(100)	4	9.1×10^{-11}

Table 2: Multiregion integration of Ne atom ($r_{max}=15.0$ a.u.)

n_r (region)					Total n_r	$\Delta\rho(r)$
1	2	3	4	5		
10	15	12	16	3(3)	56(56)	5×10^{-9}
15	20	24	24	11(16)	94(99)	1×10^{-12}

Table 3: Euler-Maclaurin integration of Cu atom ($r_{max}=22.0$ a.u.)

n_r	m_r	$\Delta\rho(r)$
47(64)	2	6.0×10^{-6}
43(64)	3	6.4×10^{-8}
40(64)	4	7.6×10^{-6}
71(96)	2	5.2×10^{-9}
64(96)	3	1.4×10^{-10}
60(96)	4	4.4×10^{-10}
95(128)	2	6.5×10^{-9}
86(128)	3	4.9×10^{-12}
80(128)	4	1.1×10^{-13}
77(128)	5	1.1×10^{-10}

Table 4: Regions for Cu atom (a.u.)

	a	m	b
1	0.000	0.005	0.010
2	0.010	0.038	0.077
3	0.077	0.170	0.380
4	0.380	0.630	0.940
5	0.940	2.500	6.000
6	6.000	—	22.000

Table 5: Multiregion integration of Cu atom ($r_{max}=22.0$ a.u.)

n _r (region)						Total n _r	Δρ(r)
1	2	3	4	5	6		
15	15	15	10	20	15(9)	84(90)	2.2x10 ⁻⁹
20	15	15	10	20	11(20)	91(100)	6.7x10 ⁻¹¹
25	20	20	15	25	11(20)	117(130)	1.4x10 ⁻¹²

Table 6: Euler-Maclaurin integration of CO molecule ($n_\theta=42$,
 radbs=1.32281,1.13383 a.u. $n_\phi=84$, $r_{max}=15.0$ a.u.). Note: same value of m_μ and m_r used for C and O.

n_r	N_{grid}	m_r	m_μ	$\Delta\rho(r)$
132,134 (192,192)	60902,62666	3	10	1.3×10^{-9}
132,134 (192,192)	60902,62666	3	11	3.0×10^{-10}
132,134 (192,192)	60902,62666	3	12	2.8×10^{-11}
132,134 (192,192)	60902,62666	3	13	9.8×10^{-12}
132,134 (192,192)	60902,62666	3	14	2.5×10^{-11}
148,150 (192,192)	87162,88926	2	10	2.1×10^{-10}
148,150 (192,192)	87162,88926	2	11	8.7×10^{-11}
148,150 (192,192)	87162,88926	2	12	3.9×10^{-11}
148,150 (192,192)	87162,88926	2	13	2.2×10^{-11}
148,150 (192,192)	87162,88926	2	14	1.6×10^{-11}
148,150 (192,192)	87162,88926	2	15	1.7×10^{-11}
124,125 (192,192)	47228,48110	4	11	8.7×10^{-9}
124,125 (192,192)	47228,48110	4	12	5.4×10^{-9}
124,125 (192,192)	47228,48110	4	13	1.8×10^{-9}
124,125 (192,192)	47228,48110	4	14	5.2×10^{-10}
124,125 (192,192)	47228,48110	4	15	1.5×10^{-9}

Table 7: Regions for CO molecule (a.u.)

	<i>a</i>	<i>m</i>	<i>b</i>
C			
1	0.00	0.025	0.05
2	0.05	0.17	0.63
3	0.63	1.27	1.90
4	1.90	4.0	6.0
5	6.0	—	15.0
O			
1	0.0	0.02	0.04
2	0.04	0.12	0.41
3	0.41	0.83	1.37
4	1.37	4.0	6.0
5	6.0	—	15.0

Table 8: Multiregion integration of CO molecule ($r_{max}=15.0$ a.u.)

n_r (region)					Total n_r	N_{grid}	m_μ	$\Delta\rho(r)$
1	2	3	4	5				
15	20	24	24	7(16)	90(99)	58078,56944	12	3.0×10^{-9}
15	20	24	24	7(16)	90(99)	58078,56944	13	1.0×10^{-10}
15	20	24	24	7(16)	90(99)	58078,56944	14	1.4×10^{-9}
15	20	24	24	9(24)	92(107)	59842,58708	13	8.3×10^{-11}
15	20	24	24	11(32)	94(115)	61606,60472	13	8.3×10^{-11}
15	20	24	32	9(24)	100(115)	66898,65764	13	5.7×10^{-11}
15	20	24	40	9(24)	108(123)	73954,72820	13	1.0×10^{-11}
15	20	24	40	9(24)	108(123)	73954,72820	12	1.4×10^{-11}
15	20	24	40	9(24)	108(123)	73954,72820	14	1.2×10^{-11}